Materials & Design 234 (2023) 112370

Contents lists available at ScienceDirect

Materials & Design

journal homepage: www.elsevier.com/locate/matdes

Microstructural refinement by spontaneous recrystallization without prior deformation of a 15-5 PH steel alloy and its mechanism

G. Ressel [a,*], D. Brandl [a], T. Hönigmann [a], M. Lukas [a], A. Stark [b], C. Gruber [c], S. Lukas [d], M. Stockinger [e], E. Kozeschnik [f]

[a] Materials Center Leoben Forschung GmbH, Roseggerstraße 12, 8700 Leoben, Austria
[b] Helmholtz-Zentrum Hereon, Institute of Materials Physics, Max-Planck-Straße 1, 21503 Geesthacht, Germany
[c] voestalpine BÖHLER Aerospace GmbH & Co KG, Mariazellerstraße 25, 8605 Kapfenberg, Austria
[d] voestalpine BÖHLER Edelstahl GmbH & Co KG, Mariazellerstraße 25, 8605 Kapfenberg, Austria
[e] Chair of Metal Forming, Montanuniversität Leoben, Franz Josef-Straße 18, 8700 Leoben, Austria
[f] Institute of Materials Science and Technology, TU Wien, Getreidemarkt 9, 1060 Wien, Austria

ARTICLE INFO

Keywords:
Recrystallization
Stainless steel
Synchrotron diffraction
EBSD
Computational thermodynamics

ABSTRACT

The recrystallization without previous deformation is reported in literature for a small, selected group of alloys. The present work provides evidence for the first time that the commercial stainless steel 15-5 PH also shows this recrystallization phenomenon during austenitization. A set of *in-situ* and *ex-situ* high-temperature techniques reveal that, on heating of the martensitic microstructure, recrystallization takes place after phase transformation between 900 and 1000 °C, causing a distinct reduction of the austenite grain size. This work also shows that the recrystallization correlates with the mechanisms involved in the prior martensite to austenite transformation. It is observed that increasing heating rates lead to decreasing grain sizes. This is attributed to increased defect density in the reverted austenite and increased driving pressure for the nucleation of recrystallized grains. It is proposed that, during martensite to austenite reversion, a defect arrangement of highly stable low-angle grain boundaries and, with increased heating rate, an increased density of internal, grown-in dislocations is inherited from martensite laths. This highly defect-loaded microstructure, formed without external plastic deformation, leads to a recrystallization at increased temperatures. The experimental results agree well with thermokinetic calculations based on the proposed defect arrangement, underpinning the mechanism of spontaneous recrystallization in 15-5 PH.

1. Introduction

The commercial alloy 15-5 PH is a so-called precipitation hardenable maraging steel and exhibits a good combination of strength, toughness, and oxidation resistance. It is typically used in structural components in aircrafts or specific conveyor systems in the industry. After a standard metallurgical production process, including several thermomechanical processing steps, solution annealing is conducted to dissolve predominantly Cu-based precipitates for subsequent precipitation hardening during tempering. In addition to the fine particle precipitation, the formation of so-called reverted-, or intragranular austenite at elevated or even high temperatures in various steel grades, such as 15-5 PH, PH13-8, soft martensitic steels, duplex steels, or Mn steels, is reported in the literature during tempering. These works claim that reverted austenite formation is accompanied by an elemental redistribution and segregation of Ni or Mn to martensite lath boundaries, retained austenite or particles, such as cementite or Cu precipitates [1–7]. At lath boundaries, this reverted austenite forms with a restricted orientation relationship (OR) to the martensitic microstructure, which is reported to be close to Kurdjumov-Sachs (KS) [8] and shows the same orientation as the previous austenite [9–11].

During further heating from tempering temperatures to austenitization temperatures, the formation of reverted austenite can be extended to a nearly complete transformation, which is, in some references, denoted as austenite memory or structural inheritance (SI) [4,12–20]. It is the complete reversion of martensite to austenite with the same grain orientation, shape, and size as the previous austenite in the transformation sequence of $\gamma \rightarrow \alpha' \rightarrow \gamma$. Nakada et al. [9] proposed that this

* Corresponding author.
E-mail address: gerald.ressel@mcl.at (G. Ressel).

https://doi.org/10.1016/j.matdes.2023.112370
Received 16 August 2023; Received in revised form 22 September 2023; Accepted 25 September 2023
Available online 27 September 2023

becomes possible due to nucleation at martensitic lath- or block boundaries in KS-OR with accompanied variant restriction caused by stress fields within martensite. While the existence of this phenomenon is evidenced and very well known, the character of this reversion is still an ongoing debate. Brandl et al. [4] also reported an austenite memory effect in 15-5 PH steel. They claimed that its formation is initially accompanied by Ni partitioning to martensitic lath boundaries, implying at least a partially diffusion-controlled formation. This mechanism is in accordance with Niessen et al. [21], proposing a diffusion-controlled two-stage transformation at comparatively low cooling rates below 0.3 Ks^{-1} in similar steel. Moszner et al. [22] proposed a split mechanism in the martensitic Fe-Mn-Pd system. Apart from a diffusion-dominated mechanism, a shift towards an interface-dominated (i.e., diffusionless) austenite formation is observed at heating rates above 3.3 Ks^{-1}.

At the same time, or following the martensite to austenite reversion, some studies report a second type of austenite that lacks austenite memory and has a smaller number of defects compared to the reverted austenite [5,9–11,18,23–27]. Depending on the steel grade, the heating rate, and the holding temperature, a parallel formation of globular austenite [5,19,27], or a recrystallization process, also denoted as spontaneous recrystallization [10,12,20,24], is described in literature. Spontaneous recrystallization is the nucleation and growth of this second type of austenite without previous deformation in the reverted austenite. The globular austenite might be an early recrystallization of the reverted austenite or, as described in [5,27], nucleation in martensite at prior austenite grain boundaries, where a variant restriction does not affect the forming austenite. All previously mentioned steels have in common that they are alloyed with Ni or Mn, elements that tend to segregate to lath boundaries or other interfaces and form a reverted austenite. Studies dealing with low-alloyed Mn-Ni-Cr steels report an early formation of globular austenite, whereas studies dealing with highly alloyed Ni-Cr report a later recrystallization. Dyachenko and Chernov [20] reported a so-called “point b” at higher temperatures than A_{c3}, which is the temperature for the recrystallization or formation of globular austenite. According to these authors, the range between A_{c3} and “point b” gets larger by a higher content of alloying elements. Generally, recrystallization can only occur in a highly defect-loaded reverted austenite, offering enough driving force. In the current literature, limited understanding is available about the materials in which the particular phenomenon of recrystallization without prior deformation occurs. Its correlation with the prior transformation of martensite into austenite as a function of the heating rate is even less investigated and understood. However, this is of great importance for modeling and correctly predicting the prior austenite grain size and the mechanical properties.

For this reason, the present work demonstrates for the first time that the commercially important steel 15-5 PH exhibits a recrystallization phenomenon during austenitization without prior deformation by combining state-of-the-art *in-situ* and *ex-situ* techniques. The dependence of the recrystallization process on the heating rate and its cause is investigated by a systematic variation of the heating rate and a defect analysis by evaluating high-temperature *in-situ* electron backscatter diffraction (EBSD) measurements as well as high-temperature *in-situ* high energy X-ray diffraction (HEXRD) measurements. Their combination with thermokinetic calculations allows for an in-depth interpretation of the physical phenomenon of spontaneous recrystallization and its correlation with the prior transformation of martensite into austenite.

1.1. Experimental and computational methods

The present work investigated a conventional 15-5 PH steel produced at voestalpine BÖHLER Edelstahl GmbH & Co KG and processed at voestalpine BÖHLER Aerospace GmbH & Co KG. Table 1 shows the chemical composition of the investigated steel.

To investigate the austenitization in 15-5 PH, *in-situ* EBSD measurements with two varying heating rates of 10 Ks^{-1} and 3.3 Ks^{-1} were performed with a Zeiss Gemini Crossbeam 340 SEM device equipped with an Oxford Instruments Symmetry EBSD detector. For these EBSD measurements, a step size of 250 nm was chosen to ensure a good compromise between low retention time during scanning and acceptable resolution. The EBSD data was evaluated using the AZtecCrystal Processing Software of Oxford instruments and its version 5.1.

Table 1
Chemical composition of pH 15-5 in wt.%.

C	Si	Mn	Cr	Ni	Cu	Nb	N
0.03	0.3	0.5	15.0	5.1	3.2	0.3	0.01

In-situ high-temperature HEXRD measurements were carried out at Deutsches Elektronen-Synchrotron (DESY) on beamline P07 at Petra III [28] operating with a photon energy of 87.1 keV, which corresponds to a wavelength of 0.142350 Å. During HEXRD measurements, specimens were heated in a TA instruments dilatometer type 805A using rates of 0.33, 3.3, and 33 K/s. For the calculations of defect densities via [29,30], the burgers vector *b* was derived for the [1 1 0] crystallographic direction by using the lattice parameter (*a*) measured by *in-situ* HEXRD measurements at respective temperatures. Data gained by HEXRD measurements were processed using an in-house programmed evaluation tool directly tailored for automated evaluation of the large amount of data produced during *in-situ* measurements.

Additional heat treatments were conducted on a TA instruments dilatometer type 805A for complimentary *ex-situ* prior austenite grain size determination. The so-produced specimens were metallographically prepared according to the procedure published in [31,32]. In these dilatometry experiments, a variation of 9 heating rates between 0.033 and 200 Ks^{-1} was conducted up to the austenitizing temperature of 1030 °C, where all were held for 0.5 h. In addition, dilatometry curves were evaluated regarding the start and finish of martensite to austenite reversion.

All thermodynamic and thermokinetic calculations of this study were carried out with the software package MatCalc [33], version 6.04.0153, with the open thermodynamic databases “mc_fe.tdb” (version 2.060) and “mc_fe.ddb” (version 2.012).

1.2. Results

1.2.1. Evidence of spontaneous recrystallization in 15-5 PH and its dependence on heat treatment parameters.

The evolution of the microstructure during heating at a rate of 10 Ks^{-1} to the austenitizing temperature of 1030 °C is shown in Fig. 1 at the same position as inverse pole figure (IPF) as well as kernel average misorientation (KAM) mappings. Fig. 1a and c represent the reconstructed prior austenite microstructure of martensite at room temperature and the formed austenite at 850 °C, respectively, whereas Fig. 1b refers to the original martensite. Comparing Fig. 1a and c, a similarity of shape and orientation between reconstructed austenite and the austenite at 850 °C is obvious, confirming the austenite memory effect in this temperature range in 15-5 PH. A detailed description of the formation mechanism of austenite memory, hereafter referred to as reverted austenite, is precisely described elsewhere [4]. When analyzing the KAM in Fig. 1d, an increased misorientation is observed at the reverted austenitic phases, implying an increased defect density. However, more detailed inspection reveals already small nucleated grains, preferably at the prior austenite grain boundaries in the form of necklace grain structures (marked by red arrows). These small grains are surrounded by reverted austenite and show significantly lower KAM values, depicted in blue, evidencing that 15-5 PH shows recrystallization after martensite to austenite reversion in Fig. 1d. Notably, this is not caused by prior deformation but apparently after the formation of the reverted austenite. The spontaneously recrystallized grains exhibit similar orientations to the original reverted austenite, suggesting a nucleation mechanism by strain-induced grain boundary migration (SIBM) of

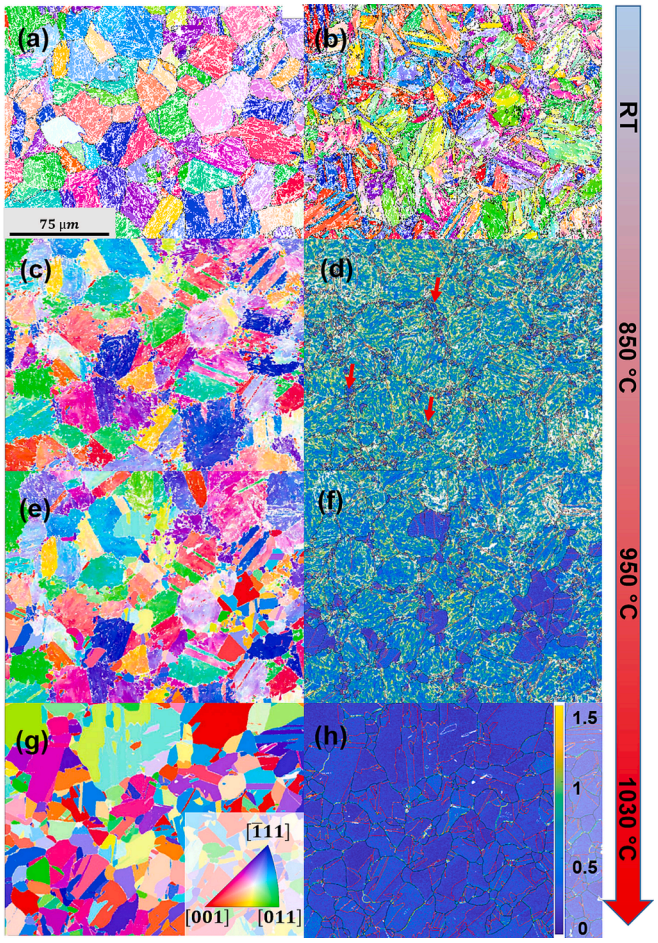

Fig. 1. *In-situ* investigation of the austenitization of 15-5 PH by high-temperature EBSD with a heating rate of 10 K/s. (a) Reconstructed austenitic microstructure at room temperature as IPF (b) IPF of the original martensitic microstructure. (c), (e) and (g) show the IPFs for austenite at temperatures 850 °C, 950 °C, and 1030 °C, respectively. (d), (f) and (h) show the corresponding KAMs at the corresponding temperatures. In (c) and (d), austenite memory is shown as austenite grain orientation and shape, being the same as the reconstructed austenite shown in (a). Its KAM in (d) shows the first small recrystallized grains marked with red arrows. Increasing the temperature provokes progress in recrystallization with a completely new and finer structure (as shown in (e) to (h)).

critical subgrains [34]. Upon further heating from 850 °C to 950 °C (Fig. 1e–f), a growth of these small recrystallized grains is discernible since, at the same positions, a higher fraction of newly formed austenite grains is found with a completely new arrangement, orientation, and shape, compared to the reverted austenite. Further increasing the temperature to 1030 °C (Fig. 1g–h) reveals an almost completely recrystallized microstructure with a new and finer appearance than the original austenitic grain structure.

This work also confirms spontaneous recrystallization by *in-situ* HEXRD measurements, shown in Fig. 2. It is evidenced, on the one hand, by the evolution of the full width at half maximum (FWHM) (solid line) and, on the other hand, by the normalized spottiness of the {200} diffraction signal (dashed line), which can also be an additional measure for recrystallization [35]. Fig. 2 depicts both as a function of temperature and heating rate (i.e., 0.33 °C/s, 3.3 °C/s, and 33 °C/s). For comparability, the difference between the FWHM value to them of the recrystallized structure (i.e. dFWHM) is shown. At all heating rates, a spontaneous drop of the FWHM at temperatures higher than 930 °C can be seen, confirming the presence of spontaneous recrystallization with lower FWHM and, thus, defect density in this temperature range.

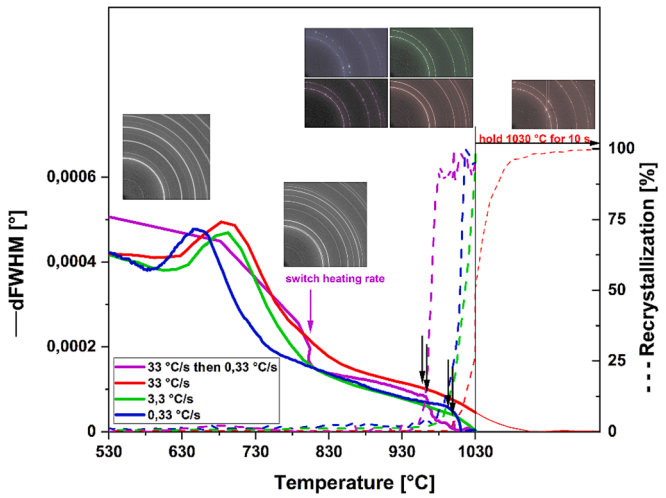

Fig. 2. Comparison of the FWHM evolution of the austenite (200) diffraction peak (solid line) as well as normalized spottiness (dashed line) of the diffraction patterns as a measure for recrystallized phase fraction of austenite for different heating rates. Whereas the red, green, and blue graphs correspond to heating rates of 33, 3.3, and 0.33 K/s, respectively, the magenta graph results from heating with 33 K/s during the formation of reverted austenite and, subsequently, heating with 0.33 K/s during recrystallization. The respective onset of recrystallization is marked with arrows. (For interpretation of the references to color in this figure, the reader is referred to the Web version of this article.).

Recrystallization is also corroborated by the increased spottiness of the diffraction pattern, as illustrated in Fig. 2. The lower FWHM after recrystallization agrees with the results of *in-situ* EBSD measurements, showing lower KAM in recrystallized austenite grains. (Note: The onset of recrystallization in EBSD is underestimated, as accelerated surface diffusion is active during this method. Thus, HEXRD measurements reveal recrystallization in the bulk of 15-5 PH and EBSD at the surface).

In order to corroborate existing *in-situ* investigations and to strengthen the understanding of the recrystallization process in reverted austenite of 15-5 PH, additional heat treatments with varying heating rates up to austenitizing temperature were carried out by dilatometry and analyzed with respect to prior austenite grain size. As shown in Fig. 3 15-5 PH shows a smaller austenite grain size after austenitization

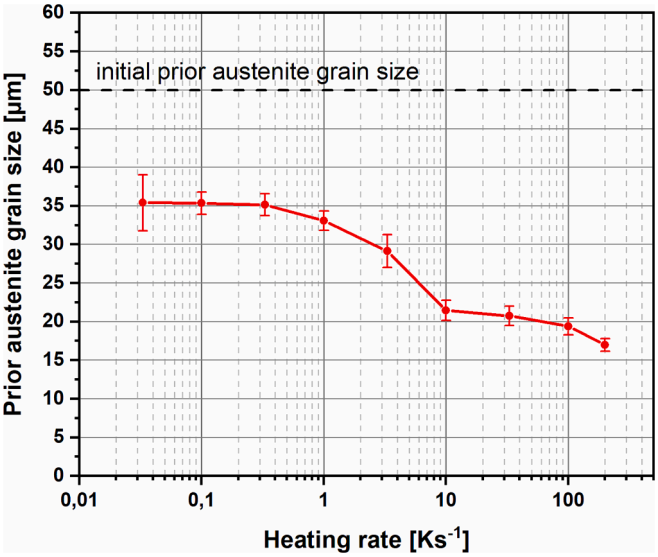

Fig. 3. Results of the heating rate-dependency of spontaneously recrystallized grain size in 15-5 PH. With an increasing heating rate, decreasing grain size is observed. The region between 1 and 10 Ks^{-1} strongly affects the grain size.

compared to the initial grain size at all heating rates, confirming the previous finding of spontaneous recrystallization. Additionally, the variation in the heating rate shows a direct correlation to the recrystallized grain size. With increasing heating rate, the recrystallized austenite grain size decreases. Further analysis reveals two plateaus of grain sizes, divided by a region between 1 and 10 Ks^{-1} of enhanced decrease of grain sizes, implying an increasing driving force for nucleation during recrystallization in this region.

Additional heat treatments with more complex time–temperature profiles were also performed by dilatometer measurements to extend the information on the behavior of 15-5 PH during the recrystallization process. Here, recrystallization was again identified by subsequent *ex-situ* grain size determination. Fig. 4a depicts the time–temperature profiles of the conducted heat treatments S1-S3. Whereas S1 corresponds to the standard heat treatment heated with a rate of 3.3 Ks^{-1} directly to the austenitization temperature of 1030 °C, S2 represents a heat treatment with an intercritical holding step at 730 °C for 1 h with subsequent heating to austenitization temperature to investigate the stability of defects in reverted austenite, affecting subsequent recrystallization. *Ex-situ* grain size evaluation in Fig. 4b showed that the refining effect of recrystallization is still operative in this condition since the grain size decreases from ~ 50 μm to ~ 24 μm. This fact confirms the presence of stable defect arrangements such as, e.g., subgrains in the reverted austenite, where annealing at 730 °C for 1 h is insufficient to suppress spontaneous recrystallization upon subsequent heating. These defects still provide enough driving force. This is underlined by the fact that holding at 730 °C in S3 and subsequent cooling to room temperature showed no grain refining effect, excluding the possibility of recrystallization already at 730 °C. Grain size determination further revealed even a smaller grain size for S2 than for S1, suggesting an increased nucleation rate in S2 compared to S1. This is probably due to increased Cr/Ni partitioning during reverted austenite formation and metastable martensite formation as well as additionally formed NbC. Arising particle-stimulated nucleation (PSN) from the metastable martensite and NbC might cause increased nucleation rates for recrystallization. In contrast, the chemical heterogeneities can also cause solute drag effects, reducing the grain boundary mobility and thus growth of spontaneously recrystallized grains.

1.2.2. Heating rate-dependency on the onset of recrystallization and defect density in reverted austenite

Since the recrystallized grain size in 15-5 PH is sensitive at heating rates between 1 and 10 Ks^{-1} (see Fig. 3), *in-situ* EBSD and HEXRD experiments were performed in this work precisely in this range. Fig. 5 and its evaluation in Table 2 compares the fraction of spontaneously recrystallized austenite of the heating rates 10 Ks^{-1} and 3.3 Ks^{-1} at different temperatures and gives an insight into the onset and kinetics of recrystallization. When comparing both heating rates, an increased amount of recrystallized grains at 850 °C is observed at a heating rate of 10 Ks^{-1} (15.4 % compared to 8.9 % at 3.3 Ks^{-1}), which can again be distinguished from the reverted austenite by its low misorientation and, thus, blue appearance in Fig. 5. This applies despite the shorter time at elevated temperatures. Additionally, at 10 Ks^{-1} heating rate, these recrystallized grains appear smaller but higher in number density.

In contrast, at 950 °C, the proportion of recrystallized grains changed, and at 3.3 Ks^{-1} an almost entirely recrystallized microstructure is present (92.2 %), whereas at 10 Ks^{-1} the proportion of recrystallized microstructure increased only slightly to 24.1 %. Consequently, *in-situ* EBSD measurements suggest an earlier onset of recrystallization with an increased nucleation rate for the 10 Ks^{-1} heating rate, but the process takes place over a wider temperature range. This is expected in thermokinetic processes, such as recrystallization. *In-situ* HEXRD measurements in Fig. 2 agree with this finding, indicating a somewhat earlier onset of recrystallization at a heating rate of 33 Ks^{-1} (marked by arrows in Fig. 2). This is further confirmed by an additional measurement in HEXRD with a split heating rate of 33 Ks^{-1} during martensite to austenite reversion up to 800 °C, followed by a low rate of 0.33 Ks^{-1} in the temperature range of spontaneous recrystallization. A comparison of its FWHM evolution in Fig. 2 with the constant heating rate of 0.33 Ks^{-1} confirms an increased FWHM and earlier onset of recrystallization by an approximately 50 °C lower temperature in this specimen. These results show a significant effect of the heating rate during reversion on the onset of recrystallization, confirming the previous assumption of a higher driving force for nucleation with increased heating rates.

Since the earlier onset of recrystallization strongly correlates with the defect density as the main driving force [36], EBSD measurements were analyzed in detail towards misorientations in reverted austenite. For KAM values in reverted austenite, recrystallized austenite with a grain orientation spread (GOS) lower than 4° was not considered. KAM and GOS evaluation, shown in Fig. 5 and Table 2, yield increased misorientation values at both temperatures up to a KAM of 3.95° and a GOS of 17° for the 10 Ks^{-1} heating rate compared to a KAM of 3.46° and GOS of 12° for 3.3 Ks^{-1}, agreeing with increased FWHM values in HEXRD measurements with increased heating rate. However, these misorientations are reduced at higher temperatures. This is shown in Fig. 5 by arrows, as, even at 10 Ks^{-1}, GOS values of certain grains in reverted austenite decrease during heating from 850 °C to 950 °C, which is also supported by the KAM values in Table 2, showing the same trend.

From these KAM values, geometrically necessary dislocation densities (denoted as ρ) to achieve the misorientations can be estimated

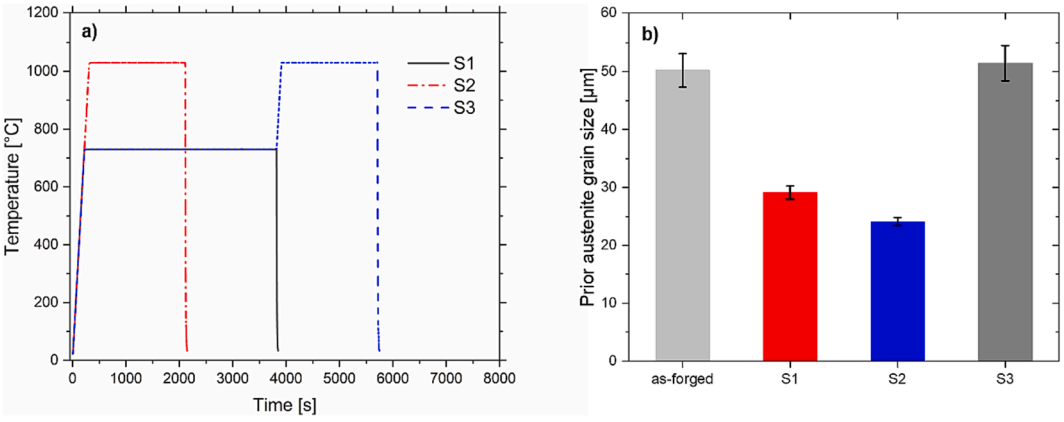

Fig. 4. Variation of heat treatments investigating the effect of defect stability against annihilation on the grain refinement caused by recrystallization. S1 shows the heat treatment investigated in Fig. 2 with heating to 1030 °C with 3.3 K/s, exhibiting a grain refinement to ~ 30 μm, whereas S2 comprised a heat treatment with a holding step at 730 °C for 1 h and subsequent heating to 1030 °C, causing the finest final recrystallized grain size of ~ 25 μm. In S3, specimens underwent a tempering at 730 °C for 1 h, exhibiting approximately the same grain size as the initial specimen.

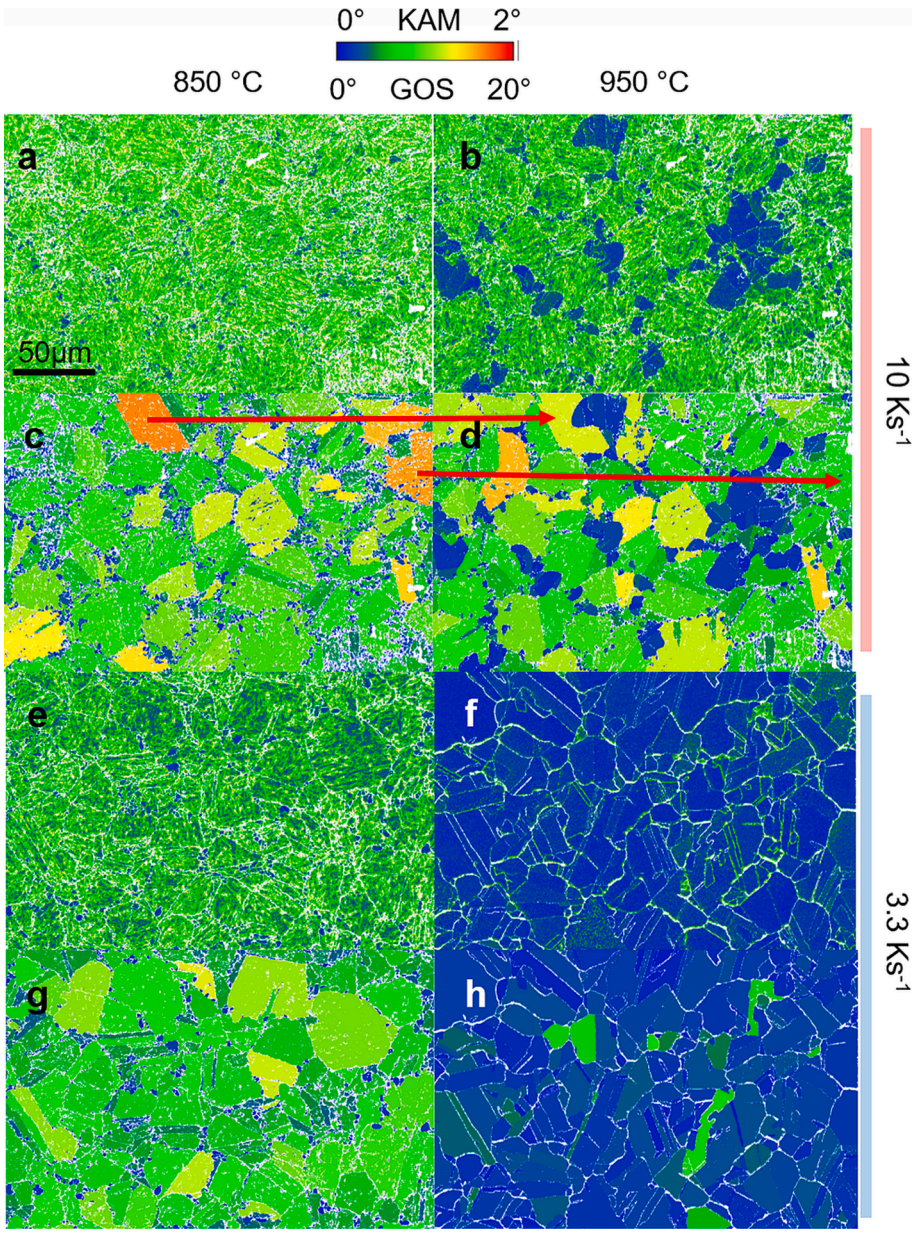

Fig. 5. KAM (a, b, e, f) and GOS (c, d, g, h) of the *in-situ* high-temperature EBSD measurements heated with a heating rate of 10 Ks^{-1} (a-d) and 3.3 Ks^{-1} (e-h) at a temperature of 850 °C (a, c, e, g) and 950 °C (b, d, f, h). Higher heating rates result in increased misorientations with the reverted austenite, implying increased defect densities. In addition, these measurements corroborate the earlier onset of recrystallization since an increased proportion (shown here in blue as they exhibit low KAM and GOS values) is present at 850 °C and a heating rate of 10 Ks^{-1}.

Table 2
Results of the evaluation of *in-situ* high-temperature EBSD measurements evidencing increased defect density in reverted austenite at a heating rate of 10 Ks^{-1} compared to 3.3 Ks^{-1}. Additionally, a higher proportion of recrystallized microstructure is found at a heating rate of 10 Ks^{-1} at 850 °C, implying an earlier onset of recrystallization.

Temperature [°C]	Heating-rate [Ks^{-1}]	fraction of recrystallized austenite (GOS < 4°) [%]	mean KAM @ unrecrystallized reverted austenite (GOS > 4°) [°]	a [m]	b (1 1 0) [m]	ρ_{mean} [m^{-2}]	$KAM_{>P99}$ [°]	$\rho_{>P99}$ [m^{-2}]	$KAM_{>P99.9}$ [°]	$\rho_{>P99.9}$ [m^{-2}]
850	3.3	8.9	0.62	$3.645{\cdot}10^{-10}$	$2.577{\cdot}10^{-10}$	$3.4{\cdot}10^{14}$	1.73	$9.4{\cdot}10^{14}$	3.46	$1.9{\cdot}10^{15}$
	10	15.4	0.85	$3.645{\cdot}10^{-10}$	$2.577{\cdot}10^{-10}$	$4.6{\cdot}10^{14}$	2.80	$1.5{\cdot}10^{15}$	3.95	$4.0{\cdot}10^{15}$
950	3.3	92.2	0.25	$3.655{\cdot}10^{-10}$	$2.585{\cdot}10^{-10}$	$1.4{\cdot}10^{14}$	1.01	$5.5{\cdot}10^{14}$	2.42	$1.3{\cdot}10^{15}$
	10	24.1	0.73	$3.655{\cdot}10^{-10}$	$2.585{\cdot}10^{-10}$	$3.9{\cdot}10^{14}$	2.24	$1.2{\cdot}10^{15}$	3.03	$3.5{\cdot}10^{15}$

according to [29,30]. Besides the KAM, the step size of EBSD measurements representing the length of the kernel (denoted as s) and the Burgers vector b are included in the following relation:

$$\rho = \frac{2 \bullet KAM}{s \bullet b} \quad (1)$$

Based on the relation (1) and the EBSD mappings, mean ρ and maximum ρ were estimated in reverted austenite and compared between heating rates and temperatures. At 850 °C, calculations yield a mean ρ of $4.6{\cdot}10^{14}$ m^{-2} and $3.4{\cdot}10^{14}$ m^{-2} for 10 Ks^{-1} and 3.3 Ks^{-1}, respectively. To emphasize the maximum local defect density, KAM and ρ beyond the 99 % and 99.9 % percentiles (in Table 2 denoted as $\rho_{>P99}$ and $\rho_{>P99.9}$) were additionally determined. Evaluation yields a highly defect-loaded microstructure at 850 °C and 10 Ks-1 with a $\rho_{>P99}$ of $1.5{\cdot}10^{15}$ m^{-2} and a $\rho_{>P99.9}$ of $4.0{\cdot}10^{15}$ m^{-2}. Comparing the results of the different heating rates suggests that the ρ of the 10 Ks^{-1} is the highest in reverted austenite. Interestingly, even $\rho_{>P99.9}$ of the 3.3 Ks^{-1} heating rate achieves $1.9{\cdot}10^{15}$ m^{-2}, in the range of materials that recrystallize at elevated temperatures. This is noteworthy since the maximum ρ values directly correlate with $\Delta\rho$ as driving pressure for recrystallization nucleation, confirming that higher heating rates produce increased $\Delta\rho$ and an earlier onset correlated with increased nucleation rates for finer recrystallized grains. As already shown previously by GOS values, ρ slightly reduces from 850 °C to 950 °C, suggesting that, during heating, defects recover in a moderate amount, thus reducing ρ. As expected, a smaller proportion of dislocations annihilates during heating with 10 Ks^{-1}, reducing, e.g., ρ_{mean} by $0.7{\cdot}10^{14}$ m^{-2}, whereas the annihilation is stronger at 3.3 Ks^{-1} with $2{\cdot}10^{14}$ m^{-2}.

From these results, it can be concluded that the defect-loading in reverted austenite increases with increasing heating rate. This affects recrystallization with an earlier onset and a higher nucleation rate, forming a finer grain structure in the end and explaining the dependence of the grain sizes on the heating rate shown in Fig. 3.

1.2.3. On the character of martensite to austenite reversion in 15-5 PH

From experimental findings in the present work, it is evident that the origin of spontaneous recrystallization is directly correlated with the mechanism and character of the martensite to austenite reversion in 15-5 PH. Fig. 6a shows the calculated driving forces for the martensite to austenite transformation and *vice versa*. The solid lines refer to the transformations with a partitioning of elements, whereas the dash-dotted lines are calculated for the diffusionless transformations (with no change in the chemical composition). The lines denoted with "cooling" represent driving forces for martensite formation from austenite. The "heating" lines correspond to the cases where reverted austenite forms within the martensite microstructure. Note that the driving forces for the case of heating-partitioning below 800 °C are shown as dashed lines because numerical problems prevented a complete equilibrium partitioning from being evaluated. The dotted line was evaluated for a constrained equilibrium case, where the chemical composition of austenite was taken to be invariable below 800 °C. In the driving force calculations, no kinetics are taken into account, which means that these calculations only deliver the temperatures at which a particular transformation becomes thermodynamically possible.

The cooling curves in Fig. 6a are relevant for the austenite to martensite transformation, and they are plotted for the sake of completeness. Mostly, the cooling-no partitioning case is of relevance since it refers to the temperature below which the martensite transformation becomes thermodynamically possible. The heating-related curves are of significantly higher relevance for the present work since they refer to the situation where reverted austenite forms during the heating of the martensite microstructure. Accordingly, the formation of partitioning reverted austenite is possible at practically all calculated temperatures, as elaborated by Brandl et al. [4] with DICTRA calculations and assuming local equilibrium at the transformation interface. However, the partitioning transformation occurs along with long-range diffusion of Cr and Ni, and it is, thus, dependent on sufficient diffusional mobility of these elements. In the previous work [4], this transformation has been proven feasible under the present conditions, at least, with low enough heating rates. Above roughly 575 °C, the thermodynamic analysis suggests that the austenite reversion is also thermodynamically possible without partitioning and, thus, without the need for long-range diffusion of Cr and Ni. The partitionless fast transformation occurs in competition with the slower diffusion-controlled reaction above this

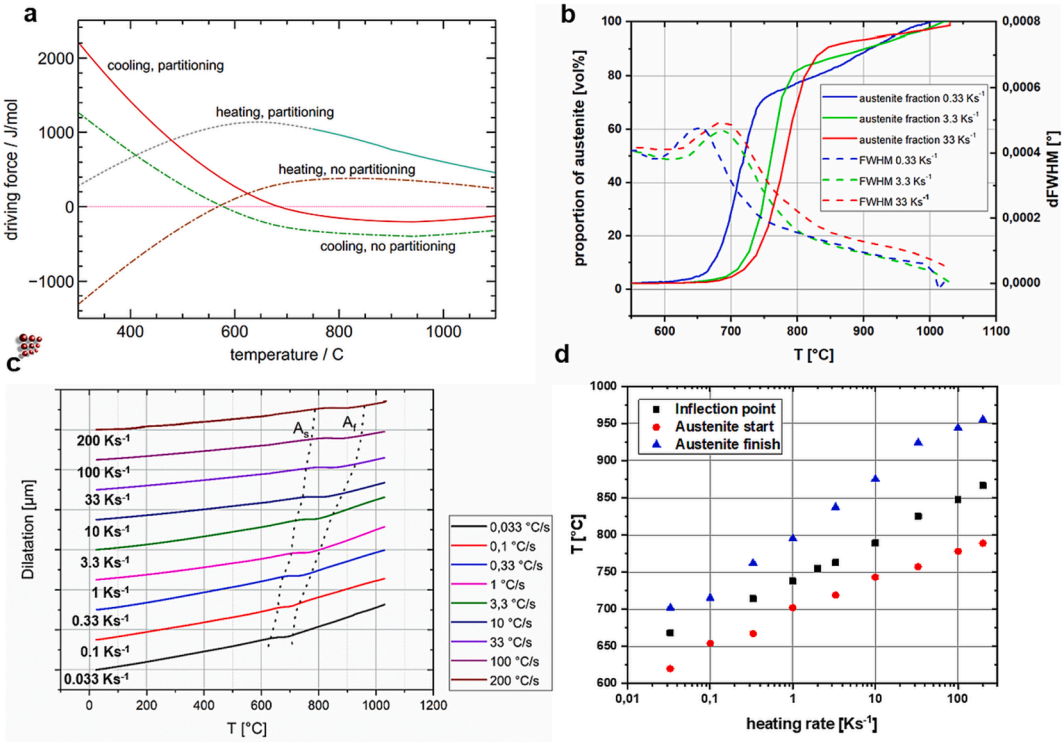

Fig. 6. Results of thermodynamic calculations revealing the driving force as a function of the temperature of a diffusion-controlled (solid lines) and diffusionless (dash-dot lines) reversion in (a), three-stage martensite to austenite reversion shown by the evolution of the austenite fraction and FWHM in (b) and depiction of the start- and finish temperatures of the second stage of reversion measured by dilatometry in (c) and (d).

temperature, which is elaborated in more detail subsequently. In any case, the thermodynamic analysis already indicates that the diffusion-controlled transformation will dominate the reversion process at temperatures below 575 °C and compete with the fast diffusionless transformation above this limit.

To get a better insight into the possible competition during the reversion process, HEXRD measurements were conducted in this work to analyze the transformation process in detail, as shown in Fig. 6b. Measurements revealed three different stages during the martensite to austenite reversion. Following the evolution of FWHM, a local maximum can be found at a temperature between 630 °C and 730 °C in all heating rates. Comparison with the austenite fraction reveals that the beginning of the increase in FWHM correlates with the beginning of the transformation. As already outlined, at lower temperatures and thus in the first stage of reversion, reverted austenite forms accompanied by a Ni/Cr partitioning and segregation of Ni to lath boundaries. The local maximum of FWHM is most likely related to the same phase fraction of retained and reverted austenite, with a maximum chemical difference in Ni and Cr content, respectively [4]. Apparently, increased heating rates lead to increased transformation temperatures, indicating a time-dependent transformation. However, with increasing heating rates, transformation temperatures converge since 33 Ks^{-1} shows only a somewhat higher transformation start temperature than 3.3 Ks^{-1}, indicating an increased athermal proportion of the transformation with increased heating rates. Subsequently, in the second stage of reversion, a substantial decrease of the FWHM is detected, representing the main transformation of approx. 75 % of martensite to reverted austenite. In this temperature range, it is assumed that the part of martensite transforms that is dominated by partitionless formation and, thus, tends to show a lower chemical difference to the martensite and melt composition. This stage is most likely the interface-dominated part of the multi-staged reversion behavior. Due to the high amount of austenite formed and its chemical homogeneity, it drastically reduces the FWHM during its formation. This also may superimpose the effect of the inheritance of defects in this stage. It is evident in Fig. 6b that the highest amount of austenite formed in this stage is formed during heating with 33 Ks^{-1}, which finally shows the highest FWHM value, indicating increased defect densities before recrystallization. Finally, in the third stage of reversion, the FWHM decreases at a much lower rate, which is accompanied by a lower rate of austenite formation. This type of austenite formation is retarded again by metastable martensite stabilized by the chemical Ni/Cr redistribution during the first stage, where Ni is depleted and Cr is enriched. Additionally, partial recovery of defects in reverted austenite might also contribute to the decrease in FWHM in a moderate amount, which is also reflected in later simulations.

When comparing transformation temperatures of the reversion revealed via HEXRD with those measured with dilatometry, shown in Fig. 6c-d, the dilatometry reveals predominantly the second stage of reversion. In general, dilatometry results confirm previous HEXRD measurements that the reversion is time-dependent at all heating rates, but the transformation temperatures converge at higher heating rates. Interestingly, the temperature span between the start and finish of the second stage increases between 1 and 10 Ks^{-1}, but stays constant below and beyond this range, indicating that, particularly between these heating rates, the amount of the second stage transformation increases. Precisely in this region, the defect density increases, and the recrystallized grain size decreases significantly, as shown in Fig. 3.

1.2.4. Simulation of recrystallization of reverted austenite without prior deformation

To corroborate experimental findings of the recrystallization phenomenon without prior deformation, thermokinetic calculations are conducted with MatCalc. For the simulation of dislocation evolution during plastic deformation, recovery, and recrystallization, several models have recently been developed and implemented in the MatCalc package, described in detail in refs. [37–41].

The original kinetic equations describing the nucleation rate of recrystallized grains on the basis of the Rayleigh distribution [42] and the evolution of mean subgrain diameter and critical size of subgrains contain two terms that will activate subgrains to act as nuclei: (i) if the mean subgrain size increases at a constant $\Delta\rho$ and (ii) if the critical size of subgrains decreases due to, e.g., increasing $\Delta\rho$. Both mechanisms can make a certain portion of undercritically-sized subgrains become overcritical and initiate recrystallization during deformation. In the present case, no external plastic deformation is involved in the thermomechanical history. Instead, based on experimental findings of this work, it is suggested that a highly defect-loaded microstructure (martensite) re-transforms into reverted austenite and inherits a certain portion of the original defects and, eventually, adds new defects due to the displacive nature of the martensite transformation to reverted austenite. This means that the simulation starts with a pre-defined microstructure, in contrast to an evolving microstructure with continuous plastic deformation. This implies that, on the one hand, (i), a predefined "subgrain size distribution" is inherited from the martensitic substructure, in the present case, approximated by the lath-thickness of the martensite. In addition, (ii), a certain fraction of dislocations is also inherited from the interior of the martensite laths. In the simulations, a constant lath thickness of 300 nm is used, in agreement with experiments [4]. As outlined later, the dislocation density of the lath interior is taken as a weak function of transformation temperature (heating rate) with values between 0.95 and $1.25{\cdot}10^{15}$ m^{-2}, the lower dislocation density values corresponding to the lower heating rates, again, in agreement with the experimental observation described in section 1.3.2.

These initial defects are accounted for in the simulations with a certain density of geometrically necessary dislocations (GNDs), which are stored in the parent martensite lath boundaries, and the internal dislocation density in the interior of the former martensite laths. The GNDs are parameterized by the misorientation angle between two subgrains and the so-called Read-Shockley dislocation density, which defines the minimum number of dislocations required to form a subgrain boundary with a misorientation angle θ. The value, which is chosen as constant in the simulations, is $\theta = 6°$. It is higher than the experimentally observed values present in martensitic lath boundaries. However, the angle θ refers to a perfectly recovered subgrain boundary, which is not present after the austenite transformation. The Read-Shockley dislocation density corresponding to $\theta = 6°$ and a subgrain size $\delta = 300$ nm is calculated [35] as ρ_{RS} $1.5 \bullet 10^{15} m^{-2}$. It will decrease during the reaction due to moderate subgrain growth/coarsening and, thus, reduce the driving force for recrystallization.

Fig. 7a shows the calculated recrystallized fractions as obtained in the simulations. The curves are in good agreement with the experiments described in section 1.3.2, where the EBSD analysis of samples heated with either 3.3 Ks^{-1} or 10 Ks^{-1} shows almost complete recrystallization at 950 °C in the slowly heated sample, while the fast-heated sample shows only a small number of recrystallized grains. Interestingly, all slowly heated samples up to 10 Ks^{-1} recrystallize already during heating and before reaching the isothermal holding temperature of 1030 °C. The calculations show that higher heating rates lead to incomplete recrystallization during heating.

While Fig. 7b shows the (spontaneously) recrystallized grain sizes as a function of time, Fig. 8a displays the recrystallized grain size as a function of heating rate after the austenitization at 1030 °C for 0.5 h. The experimental points (full red triangles) decrease from roughly 36 μm at the lowest heating rates of approx. 0.1 Ks^{-1} to 19 μm at 100 Ks^{-1}. The open square symbols connected by the green dashed line show the simulation results assuming a constant internal dislocation density with a value of $1.1{\cdot}10^{15}$ m^{-2}. They reproduce the trends in the recrystallized grain size well, although they are quantitatively incorrect. The blue solid line with the open circles represents simulations, where the initial internal dislocation density is assumed to follow the trend of the measured dislocation densities as described in section 1.3.4. Accordingly, at the lowest heating rates, a lower dislocation density is used in the

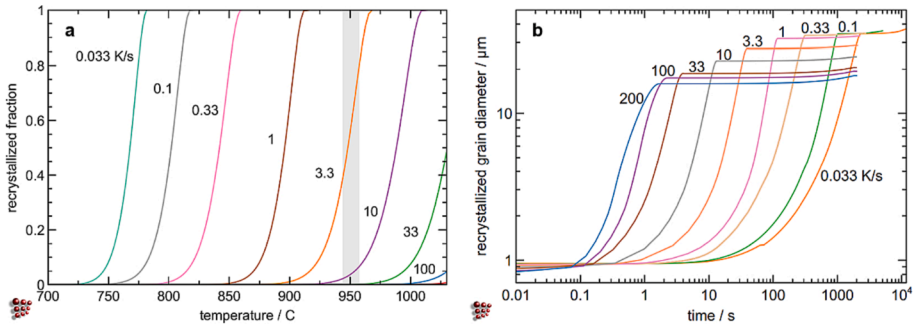

Fig. 7. Simulated recrystallized fraction (a) and mean recrystallized grain diameter (b) during heating and spontaneous recrystallization as a function of the heating rate. The grey bar marks the 950 °C region, where the degree of recrystallization has been observed as described in section 1.3.2.

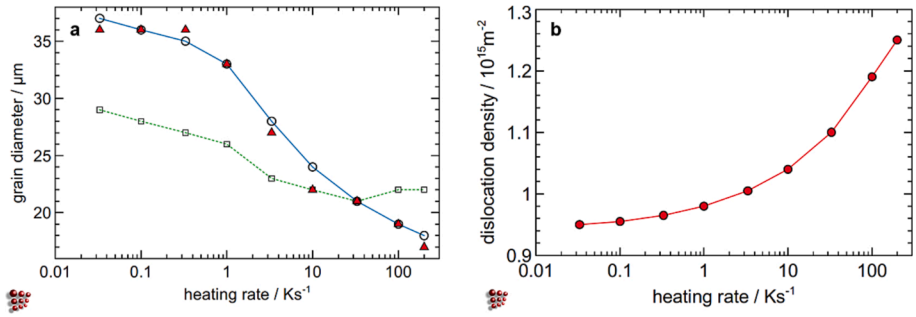

Fig. 8. Simulated recrystallized grain diameter (a) and variable internal dislocation density (b) as a function of heating rate. The square symbols in the left diagram refer to a constant internal dislocation density of $1.1{\cdot}10^{15}$ m^{-2}. In contrast, the open circles connected by the blue solid line are based on calculations with variable internal dislocation density, as shown in (b).

simulations, starting with $0.95{\cdot}10^{15}$ m^{-2} and increasing to 1.25 10^{15} m^{-2}, as shown in Fig. 8b. Interestingly, this relatively small variation in dislocation density brings the simulations into almost perfect agreement with the experimentally observed recrystallized grain sizes.

1.3. Discussion

1.3.1. Evidence of recrystallization without prior deformation in a commercial 15-5 PH

For the first time, recrystallization without prior deformation is evidenced directly by sophisticated *in-situ* high-temperature experiments in the commercial alloy 15-5 PH. After the formation of so-called reverted austenite, *in-situ* high-temperature EBSD and HEXRD measurements of this work confirm recrystallization during austenitizing to 1030 °C. The recrystallized grains exhibit a lower KAM and cause a spontaneous drop in FWHM at temperatures above 930 °C during continuous heating. Also, *ex-situ* investigations of this work in Fig. 4 confirm the presence of spontaneous recrystallization and reveal a decrease in the recrystallized austenite grain size from 50 µm to 17–35 µm. This remarkable fact is essential to note as the commercial alloy 15-5 PH is, e.g., used as material for the aerospace industry, where the control of prior austenite grain size is essential for controlling martensitic block sizes. Besides other microstructural features [43], these block sizes affect the mechanical properties, such as cleavage crack propagation of components consisting of pH steels [44]. Liu et al. [23,24] found the spontaneous recrystallization and an accompanied grain size reduction using a confocal laser scanning microscope (CLSM) at soft martensitic steel without Cu and NbC precipitates and lower Cr content. Furthermore, Tsuchiyama et al. [45,46] found this kind of recrystallization process without prior deformation also in highly defect-loaded martensite, forming recrystallized ferrite in low-alloyed ultra-low carbon steels with 1.5 wt% Mn. This also supports the presence of this phenomenon in other types of steels and phases. However, the steel investigated by Liu shows a lower onset of recrystallization than the actual 15-5 PH. This can be due to smaller microstructural sizes and increased defect densities or caused by the analyzing method. CLSM is a method investigating phase transformations at the surface of a specimen, where accelerated diffusion triggers recrystallization at lower temperatures. This is also found in the present work, where EBSD measurements at the surface indicate an earlier recrystallization as HEXRD, detecting transformations in bulk. Additionally, some studies [5,10,11,27] have found a parallel formation of so-called globular austenite at lower temperatures in lower-alloyed Mn steels, exhibiting a lower defect density than the reverted austenite. The formation of this globular austenite can also be an accelerated early recrystallization or a nucleation in martensite at prior austenite grain boundaries, where a variant restriction does not affect the austenite formation [5,27]. The onset might also correlate with the chemical composition outlined by Dyachenko [20] and Chernov [47]. These authors proposed that the range between A_{c3} and the onset of recrystallization (in their work denoted as point b) becomes more prominent by a higher content of alloying elements. This fact agrees with the findings of the present work since actual 15-5 PH shows increased onset temperatures compared to the lower-alloyed alloys in the literature. Generally, recrystallization is not affected only by alloying elements but at least by four parameters [36]. First, by the driving force represented by the stored energy and, thus, the material's local defect density difference (correlates with defect density). Second, by the mobility and ability of cross slipping of dislocations, which is a function of the stacking fault energy (SFE). Third, by the availability of nucleation sites, which also depends on the grain- and subgrain sizes as pre-existing nuclei. Fourth, by the mobility of the recrystallized grain boundaries, which is affected by temperature, misorientation, and defect density (especially internal dislocations from a different gliding system can act as pinning points of moving grain boundaries, causing a bulging in-between [48]), as well as solute- and Zener drag [36,49–51]. Apparently, after martensite to austenite reversion, 15-5 PH shows a combination of these factors, allowing for subsequent recrystallization.

Furthermore, by analyzing Fig. 1, recrystallization in 15-5 PH seems to follow the theory of SIBM [34,36,42], where subgrains beyond a critical radius act as nuclei for recrystallization, causing a bulging of high-angle grain boundaries. Exactly this can be found in Fig. 1, as grain boundaries are bulged at 850 °C, and a relation between the recrystallized orientations and the previous is implied. Bulge nucleation is also found in highly defect-loaded martensite, forming recrystallized ferrite in ultra-low carbon steels [45,46].

1.3.2. Heating-rate dependency of recrystallization and defect arrangement in reverted austenite

At least three characteristics can be found when analyzing recrystallization and the defect loading of reverted austenite as a function of heat treatment variation.

First, at all heating rates (even at the lowest with 0.033 Ks^{-1}), enough stored energy is available for recrystallization. Calculating dislocation densities from KAM values in this work yield comparatively high values between 10^{14} and 10^{15} m^{-2}, despite the fact that this method tends to underestimate the dislocation density [52]. At some local positions, defect densities beyond $1 \bullet 10^{15}$ m^{-2} are observed. This is in the range of martensitic microstructures [53] and deformed materials that are able to recrystallize [36]. In comparison, cold-worked copper with a dislocation density of 10^{15} m^{-2} exhibits a stored energy of approximately 2 MJ/m^3 leading to recrystallization [36], suggesting enough stored energy for recrystallization at these dislocation densities.

Second, even intercritical holding at 730 °C for 1 h does not reduce the defect density in a way that recrystallization is impeded. This means a certain number of dislocations remains stable, allowing for recrystallization. In literature [36,49], it is well known that the low-angle grain boundaries (LAGB) between subgrains contain dislocations in a highly stable arrangement [49]. As the reverted austenite in 15-5 PH also shows an austenite memory effect, it is suggested that this can be possible when a nucleation with a variant restriction at martensitic lath boundaries is present. With that mechanism, the misorientation angle of the martensitic laths, amounting to 4 to 5° [54,55], can be inherited to reverted austenite when they coalesce with the adjacent reverted austenite crystal. Consequently, the size of the subgrains and the misorientation angle θ of their LAGBs are mainly controlled by the nature of martensitic laths.

Third, a heating rate dependency on the defect density is observed in our investigations. Especially between 1 and 10 Ks^{-1}, the decrease in grain sizes implies an increasing driving force for nucleation during recrystallization in this region. From the dilatometer measurements, it is obvious that, exactly between these heating rates, an increase in the temperature span during the second stage of martensite to austenite reversion exists. *In-situ* HEXRD and EBSD measurements investigated this sensitive region and revealed that the martensite to austenite reversion shows increased FWHM and KAM values in the reverted austenite with increasing heating rate. Heating with 10 Ks^{-1} achieved dislocation densities up to $4 \bullet 10^{15}$ m^{-2} compared to heating with 3.3 Ks^{-1}, exhibiting dislocation densities up to $1.9 \bullet 10^{15}$ m^{-2}. HEXRD measurements confirm this trend since increased FWHM values are detected with increased heating rates. These heating rate-dependent dislocations imply an increasing displacive transformation character with increasing heating rate and are assumed to be internal, grown-in dislocations inherited from prior martensite.

Consequently, these experimental findings and their perfect agreement with thermokinetic simulations, as shown in Fig. 8, suggest the following defect arrangement in reverted austenite after martensite to austenite reversion causing spontaneous recrystallization: (i) subgrains inherited from martensite in size distribution and misorientation of martensitic laths and (ii) a varying, heating rate-dependent amount of internal dislocations.

1.3.3. Character of the martensite to austenite reversion affecting the subsequent recrystallization

As defect characteristics indicate that the origin of recrystallization is directly related to the previous martensite to austenite reversion, a detailed discussion about the character of the reversion is necessary. Thermodynamic calculations reveal that at temperatures beyond approx. 575 °C, a competition between diffusion-controlled and diffusionless transformation becomes possible. Since in all implemented heating rates, the transformation takes place beyond this temperature, it is suggested that the martensite to austenite reversion consists of a combination of both diffusion-controlled and diffusionless character. Investigation of the reversion process in more detail suggests a three-stage mechanism in 15-5 PH, representing an extension of the proposed two-staged reversion of refs. [4,21]. By considering the FWHM evolution, besides the austenite fraction, the distinction between initial formation dominated by Ni-enrichment and Cr-depletion of austenite (first stage) and subsequent reversion dominated by diffusionless formation, i.e., interface-dominated (second stage) becomes possible. This implies that the first and the third stages are primarily diffusion-dominated, whereas the second stage is interface-dominated. According to the HEXRD measurements, the proportion of the first and third stages decreases with increasing heating rate, while the proportion of the second stage increases. This underlines the increasingly interface-dominated character and the increased amount of defects inherited from highly defect-loaded martensite with increasing heating rate, as shown by FWHM and KAM values. It also agrees with the results of Brandl et al. [4], who showed an increased amount of austenite without chemical redistribution with increasing heating rates. Since, for partitioning, long-range diffusion is necessary, it is reasonable to assume that a shift toward the fast, diffusionless transformation becomes plausible. A phase transformation showing a combination of diffusion-controlled and diffusionless character is discussed as state-of-the-art in literature [22,56]. Moszner et al. [22] proposed similar findings in a Fe-Mn-Pd alloy. It is also in analogy to, e.g., the bainitic transformation as proposed by Olsen et al. [57], Bhadeshia [58], and others [59]. They proposed that diffusionless growth can occur, even when nucleation still requires some partitioning.

Furthermore, it is suggested that the phase transformation has a displacive character, characterized by an interface migration with the coordinated motion of atoms, causing additional transformation dislocations. It is also characterized by coherent or semi-coherent interfaces combined with crystallographic ORs, allowing for an inheritance of the suggested heating rate-dependent internal dislocations in martensitic laths. In literature, it is well known that a displacive transformation inherits defects from the parent phase to the child phase [26,60–62] during cooling. However, a displacive transformation is much less described in the literature during heating. Eggbauer et al. [63–65] discussed in their work an imperfect transformation from martensite to austenite during fast, inductive heating in a quenched and tempered steel, producing distorted, defect-loaded austenite and implying that even in low-alloyed carbon steel this may also be present.

1.4. Conclusion

In the present work, a sophisticated and comprehensive set of experimental and computational methods has been conducted to investigate the transformation from martensite to austenite of the commercial alloy 15-5 PH. It is demonstrated that 15-5 PH shows recrystallization without prior deformation after martensite to austenite reversion, reducing the final austenitic grain size. The presence of recrystallization is directly correlated with a three-stage martensite to austenite reversion. Depending on the stage, it is assumed that the reversion process can be subdivided into a diffusion-dominated or interface-dominated transformation. This reversion mechanism allows for defects arrangements in reverted austenite consisting of (i) LAGBs inherited from martensitic laths and (ii) internal, grown-in dislocations,

which are directly correlated with the heating rate. In 15-5 PH, the sensitive range seems to be between 1 and 10 Ks^{-1}, implying an increasing inheritance of defects and thus driving force for nucleation during recrystallization, especially in this region.

Declaration of Competing Interest

The authors declare that they have no known competing financial interests or personal relationships that could have appeared to influence the work reported in this paper.

Data availability

Data will be made available on request.

Acknowledgement

The authors gratefully acknowledge the financial support under the scope of the COMET program within the K2 Center "Integrated Computational Material, Process and Product Engineering (IC-MPPE)" (Project No 859480). This program is supported by the Austrian Federal Ministries for Climate Action, Environment, Energy, Mobility, Innovation and Technology (BMK) and for Digital and Economic Affairs (BMDW), represented by the Austrian research funding association (FFG), and the federal states of Styria, Upper Austria and Tyrol.

References

[1] R. Schnitzer, R. Radis, M. Nöhrer, M. Schober, R. Hochfellner, S. Zinner, E. Povoden-Karadeniz, E. Kozeschnik, H. Leitner, Reverted austenite in PH 13–8 Mo maraging steels, Mater. Chem. Phys. 122 (2010) 138–145, https://doi.org/10.1016/j.matchemphys.2010.02.058.

[2] L. Couturier, F. De Geuser, M. Descoins, A. Deschamps, Evolution of the microstructure of a 15–5PH martensitic stainless steel during precipitation hardening heat treatment, Mater. Des. 107 (2016) 416–425, https://doi.org/10.1016/j.matdes.2016.06.068.

[3] G. Ressel, M. Gsellmann, D. Brandl, A. Landefeld, A. Keplinger, Z.L. Zhang, V. Maier-Kiener, R. Schnitzer, Copper and its effects on microstructure and correlated tensile properties of super duplex stainless steels, Mater. Sci. Eng. A 821 (2021), 141544, https://doi.org/10.1016/j.msea.2021.141544.

[4] D. Brandl, M. Lukas, M. Stockinger, S. Ploberger, G. Ressel, Evidence of austenite memory in PH 15–5 and assessment of its formation mechanism, Mater. Des. 176 (2019), 107841, https://doi.org/10.1016/j.matdes.2019.107841.

[5] X. Zhang, G. Miyamoto, Y. Toji, S. Nambu, T. Koseki, T. Furuhara, Orientation of austenite reverted from martensite in Fe-2Mn-1.5Si-0.3C alloy, Acta Mater. 144 (2018) 601–612, https://doi.org/10.1016/j.actamat.2017.11.003.

[6] H.R. Abedi, A. Zarei-Hanzaki, M.H. Razmpoosh, A. Saboori, A.-R. Kalantari, J.-H. Cho, P. Minarik, An investigation into the reverse transformation of ferrite to austenite during friction stir processing of a duplex low-density steel, Mater. Today Commun. 35 (2023), 106386, https://doi.org/10.1016/j.mtcomm.2023.106386.

[7] P. Dastur, A. Zarei-Hanzaki, M.H. Pishbin, M. Moallemi, H.R. Abedi, Transformation and twinning induced plasticity in an advanced high Mn austenitic steel processed by martensite reversion treatment, Mater. Sci. Eng. A 696 (2017) 511–519, https://doi.org/10.1016/j.msea.2017.03.109.

[8] Y. Zhang, C. Zhang, X. Yuan, D. Li, Y. Yin, S. Li, Microstructure evolution and orientation relationship of reverted austenite in 13Cr supermartensitic stainless steel during the tempering process, Materials (Basel). 12 (2019), https://doi.org/10.3390/ma12040589.

[9] N. Nakada, T. Tsuchiyama, S. Takaki, S. Hashizume, Variant Selection of Reversed Austenite in Lath Martensite, ISIJ Int. 47 (2007) 1527–1532, https://doi.org/10.2355/isijinternational.47.1527.

[10] Y. Tomota, W. Gong, S. Harjo, T. Shinozaki, Reverse austenite transformation behavior in a tempered martensite low-alloy steel studied using in situ neutron diffraction, Scr. Mater. 133 (2017) 79–82, https://doi.org/10.1016/j.scriptamat.2017.02.017.

[11] T. Shinozaki, Y.o. Tomota, T. Fukino, T. Suzuki, Microstructure Evolution during Reverse Transformation of Austenite from Tempered Martensite in Low Alloy Steel, ISIJ Int. 57 (3) (2017) 533–539.

[12] T. Maki, H. Morimoto, I. Tamura, Recrystallization of reversed austenite and subsequent martensitic transformation in 18% Ni maraging steel, Trans. Iron Steel Inst. Japan. 20 (1980) 700–706, https://doi.org/10.2355/isijinternational1966.20.700.

[13] U.K. Viswanathan, S. Banerjee, R. Krishnan, Effects of aging on the microstructure of 17–4 PH stainless steel, Mater. Sci. Eng. 104 (1988) 181–189, https://doi.org/10.1016/0025-5416(88)90420-X.

[14] S. Watanabe, T. Kunitake, On the Formation of Austenite Grains from Prior Martensitic Structure Seiichi WATANABE and Tatsuro KITNITAKE Synopsis : Electron microscopic studies have been made of austenite partially transformed from prior martensitic structure in the temperature rang, (n.d.).

[15] A. Alaei, H. Jafarian, A.R. Eivani, Observation austenite memory and significant enhancement of tensile properties during cyclic reverse martensite transformation in a Fe-Ni-C TRIP steel, Mater. Sci. Eng. A 676 (2016) 342–350, https://doi.org/10.1016/j.msea.2016.09.003.

[16] C.N. Hsiao, C.S. Chiou, J.R. Yang, Aging reactions in a 17–4 PH stainless steel, Mater. Chem. Phys. 74 (2002) 134–142, https://doi.org/10.1016/S0254-0584(01)00460-6.

[17] S.T. Kimmins, D.J. Gooch, Austenite memory effect in 1Cr-1Mo-0·75V(Ti, B) steel, Met. Sci. 17 (1983) 519–532, https://doi.org/10.1179/030634583790420484.

[18] B.K. Sokolov, V.D. Sadovskii, Mechanism of austenite formation in heating steel, Met. Sci. Heat Treat. 1 (5) (1959) 7–14.

[19] M. Sharma, W. Bleck, Study of Structural Inheritance of Austenite in Nb-Microalloyed 18CrNiMo7–6 Steel, Steel Res. Int. 89 (2018) 1–15, https://doi.org/10.1002/srin.201800107.

[20] S.S. D'yachenko, Heredity in phase transformations: Mechanism of the phenomenon and effect on the properties, Met. Sci. Heat Treat. 42 (2000) 122–127, https://doi.org/10.1007/bf02471324.

[21] F. Niessen, M. Villa, J. Hald, M.A.J. Somers, Kinetics analysis of two-stage austenitization in supermartensitic stainless steel, Mater. Des. 116 (2017) 8–15, https://doi.org/10.1016/j.matdes.2016.11.076.

[22] F. Moszner, E. Povoden-Karadeniz, S. Pogatscher, P.J. Uggowitzer, Y. Estrin, S.S. A. Gerstl, E. Kozeschnik, J.F. Löffler, Reverse $\alpha' \rightarrow \gamma$ transformation mechanisms of martensitic Fe-Mn and age-hardenable Fe-Mn-Pd alloys upon fast and slow continuous heating, Acta Mater. 72 (2014) 99–109, https://doi.org/10.1016/j.actamat.2014.03.032.

[23] L. Liu, Z.G. Yang, C. Zhang, Effect of retained austenite on austenite memory of a 13% Cr-5% Ni martensitic steel, J. Alloy. Compd. 577 (2013) S654–S660, https://doi.org/10.1016/j.jallcom.2012.04.021.

[24] L. Liu, Z.G. Yang, C. Zhang, W.B. Liu, An in situ study on austenite memory and austenitic spontaneous recrystallization of a martensitic steel, Mater. Sci. Eng. A 527 (2010) 7204–7209, https://doi.org/10.1016/j.msea.2010.07.083.

[25] K. Nakazawa, Y. Kawabe, S. Muneki, Grain refinement of high-strength maraging steels through cyclic heat treatment, Mater. Sci. Eng. 33 (1978) 49–56, https://doi.org/10.1016/0025-5416(78)90152-0.

[26] H. Shirazi, G. Miyamoto, S. Hossein Nedjad, T. Chiba, M. Nili Ahmadabadi, T. Furuhara, Microstructure evolution during austenite reversion in Fe-Ni martensitic alloys, Acta Mater. 144 (2018) 269–280, https://doi.org/10.1016/j.actamat.2017.10.068.

[27] X. Zhang, G. Miyamoto, T. Kaneshita, Y. Yoshida, Y. Toji, T. Furuhara, Growth mode of austenite during reversion from martensite in Fe-2Mn-1.5Si-0.3C alloy: A transition in kinetics and morphology, Acta Mater. 154 (2018) 1–13, https://doi.org/10.1016/j.actamat.2018.05.035.

[28] N. Schell, R.V. Martins, F. Beckmann, H.U. Ruhnau, R. Kiehn, A. Schreyer, The High Energy Materials Science Beamline at PETRA III, Mater. Sci. Forum 571–572 (2008) 261–266, https://doi.org/10.4028/www.scientific.net/MSF.571-572.261.

[29] A. Ramazani, K. Mukherjee, A. Schwedt, P. Goravanchi, U. Prahl, W. Bleck, Quantification of the effect of transformation-induced geometrically necessary dislocations on the flow-curve modelling of dual-phase steels, Int. J. Plast 43 (2013) 128–152, https://doi.org/10.1016/j.ijplas.2012.11.003.

[30] L.P. Kubin, A. Mortensen, Geometrically necessary dislocations and strain-gradient plasticity: A few critical issues, Scr. Mater. 48 (2003) 119–125, https://doi.org/10.1016/S1359-6462(02)00335-4.

[31] D. Brandl, L. Höfler, M. Stockinger, S. Ploberger, S. Marsoner, G. Ressel, Presentation and verification of an electrolytic etching technique for the determination of prior austenite grain boundaries in the steel PH15-5, Prakt. Metallogr. Metallogr. 55 (2018), https://doi.org/10.3139/147.110497.

[32] T. Hönigmann, D. Brandl, M. Stockinger, C. Gruber, F. Frois, G. Ressel, Determination of prior austenite grain- and martensitic substructure size from metallographic etchings using a multi-step image processing algorithm Größenbestimmung von ehemaligen Austenitkörnern und martensitischen Substrukturen mit Hilfe eines mehrstuf, 59 (2022) 386–404.

[33] E. Kozeschnik, Mean-Field Microstructure Kinetics Modeling, in, Encycl. Mater. Met. Allloys, Elsevier (2022) 521–526, https://doi.org/10.1016/B978-0-12-819726-4.00055-7.

[34] J.E. Bailey, P.B. Hirsch, The recrystallization process in some polycrystalline metals, Proc. R. Soc. London. Ser. A. Math. Phys. Sci. 267 (1962) 11–30, https://doi.org/10.1098/rspa.1962.0080.

[35] M. Moreno, J. Teixeira, G. Geandier, J.C. Hell, F. Bonnet, M. Salib, S.Y.P. Allain, Real-time investigation of recovery, recrystallization and austenite transformation during annealing of a cold-rolled steel using high energy X-ray diffraction (HEXRD), Metals (basel). 9 (2019), https://doi.org/10.3390/met9010008.

[36] F.J. Humphreys, M. Hatherly, Recrystallization and Related Annealing Phenomena, second ed., Elsevier Ltd., Oxford, 2004.

[37] H. Buken, P. Sherstnev, E. Kozeschnik, Modeling the interaction between precipitation and static Recrystallization in micro-alloyed steel, in: PTM 2015 - Proc. Int. Conf. Solid-Solid Phase Transform. Inorg. Mater. 2015, 2015: pp. 913–914.

[38] H. Buken, E. Kozeschnik, Modeling Static Recrystallization in Al-Mg Alloys, Metall. Mater. Trans. A 52 (2021) 544–552, https://doi.org/10.1007/s11661-020-06100-9.

[39] H. Buken, P. Sherstnev, E. Kozeschnik, A state parameter-based model for static recrystallization interacting with precipitation, Model. Simul. Mater. Sci. Eng. 24 (2016) 35006, https://doi.org/10.1088/0965-0393/24/3/035006.

[40] H. Buken, E. Kozeschnik, A Model for Static Recrystallization with Simultaneous Precipitation and Solute Drag, Metall. Mater. Trans. A 48 (2017) 2812–2818, https://doi.org/10.1007/s11661-016-3524-5.
[41] H. Buken, S. Zamberger, E. Kozeschnik, A model for the influence of micro-alloying elements on static recrystallization of austenite, Proc. 6th Int. Conf. Recryst. Grain Growth, ReX GG 2016. (2016) 113–118. 10.1007/978-3-319-48770-0_16.
[42] M.K. Rehman, H.S. Zurob, A novel approach to model static recrystallization of austenite during hot rolling of Nb microalloyed steel. Part I: Precipitate-free case, Metall. Mater. Trans. A 44 (2013) 1862–1871, https://doi.org/10.1007/s11661-012-1526-5.
[43] A. Rosenauer, D. Brandl, G. Ressel, S. Lukas, S. Monschein, M. Stockinger, R. Schnitzer, Materials Science & Engineering A Influence of delta ferrite on the impact toughness of a PH 13–8 Mo maraging steel, Mater. Sci. Eng. A 856 (2022), 144024, https://doi.org/10.1016/j.msea.2022.144024.
[44] A. Chatterjee, A. Ghosh, A. Moitra, A.K. Bhaduri, R. Mitra, D. Chakrabarti, The role of crystallographic orientation of martensitic variants on cleavage crack propagation, Philos. Mag. Lett. under Revi (2016) 1–18.
[45] T. Tsuchiyama, Y. Miyamoto, S. Takaki, Recrystallization of Lath martensite with bulge nucleation and growth mechanism, ISIJ Int. 41 (2001) 1047–1052, https://doi.org/10.2355/isijinternational.41.1047.
[46] T. Tsuchiyama, M. Natori, N. Nakada, S. Takaki, Conditions for grain boundary bulging during tempering of lath martensite in ultra-low carbon steel, ISIJ Int. 50 (2010) 771–773, https://doi.org/10.2355/isijinternational.50.771.
[47] D.K. Chernov, Selected Works on Metallury and Metal Science [in Russian], Moscow, 1983.
[48] M. Winning, A.D. Rollett, G. Gottstein, D.J. Srolovitz, A. Lim, L.S. Shvindlerman, Mobility of low-angle grain boundaries in pure metals, Phil. Mag. 90 (2010) 3107–3128, https://doi.org/10.1080/14786435.2010.481272.
[49] T. Read, W. Shockley, Dislocation Models of Crystal Grain Boundaries, Phys. Rev. 78 (1950) 275.
[50] H.P. Stüwe, Driving and dragging forces in recrystallization, in: F. Haessner (Ed.), Recryst. Met. Mater., Dr, Riederer Verlag BmbH, Stuttgart, 1978, pp. 11–21.
[51] H. Smith, D.R.F. West, The reversion of martensite to austenite in certain stainless steels, J. Mater. Sci. 8 (1973) 1413–1420, https://doi.org/10.1007/BF00551664.
[52] J. Jiang, T.B. Britton, A.J. Wilkinson, Measurement of geometrically necessary dislocation density with high resolution electron backscatter diffraction: Effects of detector binning and step size, Ultramicroscopy 125 (2013) 1–9, https://doi.org/10.1016/j.ultramic.2012.11.003.
[53] F. Christien, M.T.F. Telling, K.S. Knight, Neutron diffraction in situ monitoring of the dislocation density during martensitic transformation in a stainless steel, Scr. Mater. 68 (2013) 506–509, https://doi.org/10.1016/j.scriptamat.2012.11.031.
[54] J.G. Back, G. Engberg, Investigation of parent austenite grains from Martensite Structure Using EBSD in a Wear Resistant steel, Materials (Basel). 10 (2017), https://doi.org/10.3390/ma10050453.
[55] S. Morito, X. Huang, T. Furuhara, T. Maki, N. Hansen, The morphology and crystallography of lath martensite in alloy steels, Acta Mater. 54 (2006) 5323–5331, https://doi.org/10.1016/j.actamat.2006.07.009.
[56] M. Hillert, Phase Equilibria, Phase Diagrams and Phase Transformations, Cambridge University Press (2007), https://doi.org/10.1017/CBO9780511812781.
[57] G.B. Olson, H.K.D.H. Bhadeshia, M. Cohen, Coupled diffusional/displacive transformations, Acta Metall. 37 (1989) 381–390, https://doi.org/10.1016/0001-6160(89)90222-8.
[58] H.K.D.H. Bhadeshia, Bainite in Steels, Third Edit, Maney Publishing, 2015.
[59] T. Klein, C. Hofer, M. Lukas, T. Wojcik, R. Schnitzer, M. Galler, G. Ressel, Formation of “carbide-free zones” resulting from the interplay of C redistribution and carbide precipitation during bainitic transformation, Materialia. 7 (2019), 100380, https://doi.org/10.1016/j.mtla.2019.100380.
[60] J.S. Bowles, D.P. Dunne, The Crystallographic Theory of Martensitic Transformations, Met. Sci. 7 (2010) 118–120, https://doi.org/10.1179/030634573790445686.
[61] G. Krauss, Steels - Processing, Structure and Performance, 2nd ed., ASM International, Ohiody, 2015. 10.31399/asm.tb.spsp2.9781627082655.
[62] N. Nakada, T. Tsuchiyama, S. Takaki, D. Ponge, D. Raabe, Transition from diffusive to displacive austenite reversion in low-alloy steel, ISIJ Int. 53 (12) (2013) 2275–2277.
[63] A. Eggbauer, M. Lukas, P. Prevedel, M. Panzenböck, G. Ressel, R. Ebner, Effect of Initial Microstructure, Heating Rate, and Austenitizing Temperature on the Subsequent Formation of Martensite and Its Microstructural Features in a QT Steel, Steel Res. Int. 90 (2019) 1–8, https://doi.org/10.1002/srin.201800317.
[64] A. Eggbauer, M. Lukas, G. Ressel, P. Prevedel, F. Mendez-Martin, J. Keckes, A. Stark, R. Ebner, In situ analysis of the effect of high heating rates and initial microstructure on the formation and homogeneity of austenite, J. Mater. Sci. 54 (2019) 9197–9212, https://doi.org/10.1007/s10853-019-03527-3.
[65] A.E. Vieweg, G. Ressel, P. Raninger, P. Prevedel, S. Marsoner, R. Ebner, Comparing fast inductive tempering and conventional tempering: Effects on microstructure and mechanical properties, Metall. Res. Technol. 115 (2018), https://doi.org/10.1051/metal/2018015.